JACS
JOURNAL OF THE AMERICAN CHEMICAL SOCIETY
pubs.acs.org/JACS
Article

UCN@C_s(6)-C_{82}: An Encapsulated Triangular UCN Cluster with Ambiguous U Oxidation State [U(III) versus U(I)]

Qingyu Meng,[‖] Laura Abella,[‖] Wei Yang,[‖] Yang-Rong Yao, Xinye Liu, Jiaxin Zhuang, Xiaomeng Li, Luis Echegoyen, Jochen Autschbach,* and Ning Chen*

Cite This: J. Am. Chem. Soc. 2021, 143, 16226−16234

Read Online

ACCESS | Metrics & More | Article Recommendations | Supporting Information

ABSTRACT: Understanding the chemical behavior of actinide elements is essential for the effective management and use of actinide materials. In this study, we report an unprecedented η^2 (side-on) coordination of U by a cyanide in a UCN cluster, which was stabilized inside a C_{82} fullerene cage. UCN@C_s(6)-C_{82} was successfully synthesized and fully characterized by mass spectrometry, single crystal X-ray crystallography, cyclic voltammetry, spectroscopy, and theoretical calculations. The bonding analysis demonstrates significant donation bonding between CN^- and uranium, and covalent interactions between uranium and the carbon cage. These effects correlate with an observed elongated cyanide C−N bond, resulting in a rare case where the oxidation state of uranium shows ambiguity between U(III) and U(I). The discovery of this unprecedented triangular configuration of the uranium cyanide cluster provides a new insight in coordination chemistry and highlights the large variety of bonding situations that uranium can have.

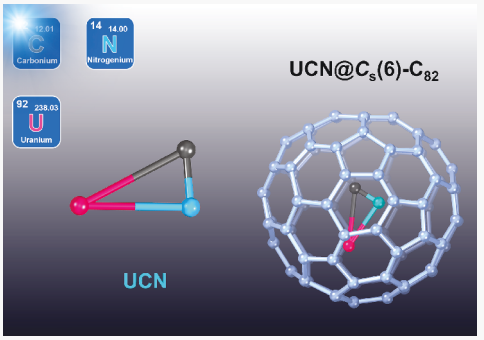

INTRODUCTION

The study of actinide clusters and gas-phase molecules provided important fundamental knowledge of the bonding behavior of actinides.[1−3] However, while actinide gas-phase molecules and clusters were widely investigated by combined spectroscopic and theoretical methods, the systematic characterization of their bonding motifs is still extremely challenging as these species are generally not stable under ambient conditions and can hardly be obtained on a macroscopic scale. Interestingly, our recent discovery of a novel endohedral fullerene family, actinide clusterfullerenes, shows that fullerene cages can be utilized as effective nanocontainers to stabilize and study rare and reactive actinide clusters, which contain unique actinide metal−ligand bonding motifs.[4−6] For example, the first reported actinide clusterfullerene, U_2C@I_h(7)-C_{80} contained a bent U═C═U cluster with two axial U═C double bonds, a bonding structure never observed in molecular compounds.[6] A study of U_2C_2@I_h(7)-C_{80} showed that it was the first molecule featuring a bonding motif with two U centers bridged by a C≡C unit.[4] These results showed that usual actinide bonding motifs can be stabilized and obtained in macroscopic quantities as endohedral clusters inside fullerene cages. Thus, the continuing exploration of novel actinide clusterfullerenes not only expands the research area of fullerene chemistry but also, more importantly, deepens our understanding of additional bonding motifs that actinides can exhibit.

CN^- is one of the most common ligands in coordination chemistry. Due to its strong coordination ability, it can stabilize various oxidation states of different metals and adopt different bonding patterns, thus providing a rich variety of compounds with different structures and physicochemical properties.[7] Therefore, the study of uranium cyanide complexes is essential for a comprehensive understanding of the 5f and 6d orbital participation in actinide−ligand multiple bonds. To date, several uranium complexes with CN^- ligands have been reported, including CN^- ligand bridging,[8−10] carbon bonding to the uranium center (UCN),[8,11−14] and nitrogen bonding to the uranium center (UNC).[13] All of the uranium cyanide complexes reported so far adopt these two coordination modes and show a near-linear configuration.

Fullerene cages were also found to be capable of stabilizing metal−cyanide clusters. Monometallic cyanide clusterfullerene (CYCF), YCN@C_s(6)-C_{82}, was first reported by Yang and coworkers in 2013.[15] So far, a series of lanthanide based CYCFs have been synthesized, isolated, and characterized, including MCN@C_{2v}(19138)-C_{76} (M = Y, Tb, and Lu),[16,17] YCN@C_s(6)-C_{82},[15] MCN@C_{84} (M = Y, Tb, Dy),[18] and MCN@C_{82}

Received: July 19, 2021
Published: September 23, 2021

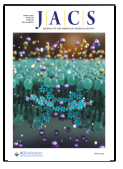

https://doi.org/10.1021/jacs.1c07519
J. Am. Chem. Soc. 2021, 143, 16226−16234

(M = Tb, Lu, and Dy).[16,19−21] One exceptional feature of the encapsulated MCN clusters is their structural flexibility, which can exist as either triangular or nearly linear geometries inside different fullerene cages.[16−21] Thus, it is intriguing to explore the possibility of entrapping an actinide cyanide cluster into a fullerene cage, which could lead to new understanding for the binding modes of cyanide with actinide ions.

Herein, we report the successful synthesis, isolation, and characterization of the first actinide cyanide fullerene, UCN@$C_s(6)$-C_{82}. UCN@$C_s(6)$-C_{82} was fully characterized by mass spectrometry, single-crystal X-ray crystallography, UV−vis−NIR, cyclic voltammetry, Raman spectroscopy, and theoretical calculations. The results show that UCN@$C_s(6)$-C_{82} can be described as a two-electron transfer from the UCN cluster to the C_{82} cage, which results formally in an open-shell electronic structure $[U^{3+}(CN)^-]^{2+}@[C_s(6)\text{-}C_{82}]^{2-}$. An unprecedented triangular UCN cluster was found in UCN@$C_s(6)$-C_{82}, which has never been observed for the traditional U-based cyanide complexes. Theoretical analyses were conducted to further understand the unique bonding nature of the triangular UCN cluster and the somewhat ambiguous oxidation state of U.

RESULTS AND DISCUSSION

Synthesis and Isolation of UCN@C_{82}. UCN@C_{82} was synthesized by a modified Krätschmer−Huffman direct-current arc-discharge method. Briefly, graphite rods, packed with U_3O_8 and graphite powder (molar ratio of U/C = 1:30), were reduced under a N_2 atmosphere at 1273 K and vaporized in the arcing chamber under a 200 Torr He and 4 Torr N_2 atmosphere. The collected soot, containing U-based endohedral fullerenes, was extracted by CS_2 for 12 h. Isolation and purification of UCN@C_{82} were performed by combined multistage HPLC procedures (Figure S1) and initially characterized by positive-ion mode matrix-assisted laser desorption/ionization time-of-flight (MALDI-TOF) mass spectrometry. The pure sample was confirmed by a single peak observed in the HPLC. The positive-ion mode MALDI-TOF mass spectrum was used to detect the purified UCN@C_{82} that shows a peak at m/z = 1248.151, and the experimental isotopic distribution agrees well with the theoretical prediction (Figure 1).

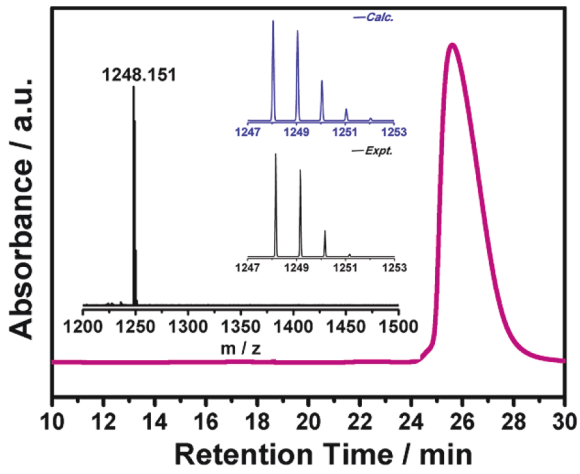

Figure 1. HPLC chromatogram of purified UCN@C_{82} on a Buckyprep-M column with toluene as the eluent. HPLC conditions: λ = 310 nm; flow rate = 4 mL/min. The insets show the positive-ion mode MALDI-TOF mass spectra and expansions of the corresponding experimental isotopic distribution of the compound in comparison with the calculated one.

Molecular and Electronic Structure of UCN@$C_s(6)$-C_{82}. Black block cocrystals of UCN@C_{82} with Ni^{II}(OEP) (OEP = octaethylporphyrin dianion), UCN@$C_s(6)$-C_{82}·[Ni^{II}(OEP)]·$2C_6H_6$, were obtained by the slow diffusion of a benzene solution of [Ni^{II}(OEP)] into a CS_2 solution of UCN@C_{82}. As shown in Figure 2a, the molecular structure was solved in the monoclinic space group $C2/m$ and unambiguously determined as UCN@$C_s(6)$-C_{82} by single-crystal X-ray diffraction analysis, excluding other molecular structures with the same molecular mass, such as U@C_{83}N and C_{120}. The shortest Ni-cage distance was measured as 2.860 Å, indicating a strong $\pi-\pi$ interaction between UCN@$C_s(6)$-C_{82} and Ni^{II}(OEP).

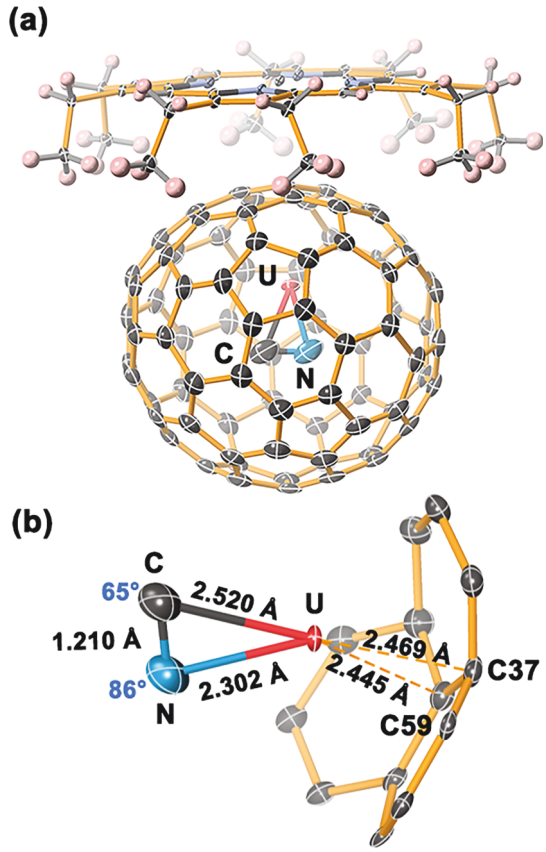

Figure 2. (a) Oak ridge thermal ellipsoid plot (ORTEP) drawing of UCN@$C_s(6)$-C_{82}·[Ni^{II}(OEP)] with 15% thermal ellipsoids. Only the major U site is shown. For clarity, the solvent molecules and minor metal sites are omitted. (b) Structural parameters of the UCN cluster. Color code: gray for C, pick for H, blue for N, white for Ni, and red for U.

In the crystal of UCN@$C_s(6)$-C_{82}, the whole molecule, including the fullerene cage and the encapsulated cluster, shows two equivalent orientations with the same occupancy of 0.5, which is common in many analogous metallofullerene/Ni^{II}(OEP) (OEP = 2,3,7,8,12,13,17,18-octaethylporphin dianion) cocrystal systems. These two equivalent orientations are mirror-related, due to the crystallographic mirror plane of the space group of $C2/m$, as shown in Figure S2. On the other hand, the encapsulated U ion shows some disordered sites, i.e., U1, U2, U3, U4, and U5, likely due to its rotational and vibrational movements. The total occupancy for U1−U5 is 0.5, and U1 is assigned as the major U site as it has a much higher occupancy of 0.324, compared to those of the other four sites (0.070, 0.0551, 0.0307, and 0.0202 for U2−U5, respectively).

https://doi.org/10.1021/jacs.1c07519
J. Am. Chem. Soc. 2021, 143, 16226−16234

Furthermore, U1A, U2A, U3A, U4A, and U5A are also generated via their mirror-related counterparts, U1, U2, U3, U4, and U5, due to the same crystallographic mirror plane. Even though U1 can be possibly assigned as the optimized U site due to its highest occupancy, U1 and U1A still need to be paired with the two mirror-related cage orientations, respectively. As the two sites (U1 and U1A) and the two cage orientations are both mirror-related and equivalent, respectively, to simplify the process, only one of the two equivalent cage orientations was selected to pair with U1 or U1A for further structural analysis (Figure S3).

The U1 is located close to a three-hexagon motif, with the shortest metal−cage distances of 2.445 Å (U1−C59) and 2.469 Å (U1−C37). The mirror-related counterpart, U1A, is located near a motif with a pentagon and two hexagon, and the closest cage carbons to the metal are C2 and C3, with distances of 2.407 and 2.391 Å, respectively (Figure S3). However, neither U1 nor U1A can be assiged as the optimal site only by crystallographic analysis bacause either of them could be safely excluded due to their similar metal−cage distances. Therefore, theoretical calculations were employed to further determine the optimized position of the encapsulated U ion relative to the selected cage orientation. DFT optimizations of the structures of U1 and U1A, i.e., structures labeled as 1 and 2, respectively (see Figure 3), indicated that the U1 site is about 23 kcal·

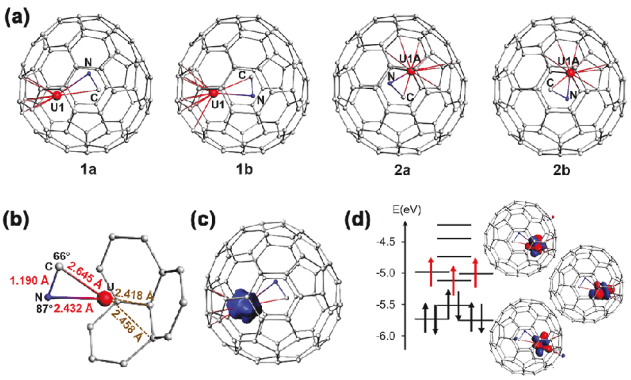

Figure 3. (a) DFT-optimized structures of UCN@C_s(6)-C_{82} with different U sites (1a and 1b to U1, 2a and 2b to U1A) and different CN relative positions. (b) Structural parameters for the spin-quartet optimized UCN@C_s(6)-C_{82} geometry. (c) Isosurface (±0.02) of the spin density for the optimized spin-quartet GS structure of UCN@C_s(6)-C_{82} at ZORA/PBE/TZP/D3 level. (d) Partial molecular orbital (MO) diagram obtained with ZORA/PBE/TZP/D3 for the ground spin-quartet state of UCN@C_s(6)-C_{82}. The singly occupied molecular orbitals (for α-spin) are drawn in red, and the associated MO isosurfaces (±0.04 au) are shown on the side. Paired electrons are drawn to denote levels with both the α and β components occupied. The energy scale corresponds to the α-spin levels. For (b), (c), and (d) the geometry of UCN@C_s(6)-C_{82} is 1a.

mol^{-1} lower in energy than U1A (Table S1). Therefore, we assign U1 as the optimal position. The U ion is over an *s*-indacene-type hexagon with the shortest metal−cage distances between 2.445 Å and 2.740 Å (Table S5). Interestingly, the U ion is also located in the symmetric plane of the C_s(6)-C_{82} cage.

It is worth noting that X-ray single-crystal diffraction alone can not reliably distinguish the N and C sites in the UCN cluster, as pointed out by previous studies,[15,19,20] due to their similar atomic size and scattering power. However, since the electronegativity of the N atom is higher than that of the C atom, the covalent interaction between the metal and the N atom is stronger in the CYCFs, resulting in a shorter M−N distance than M−C (M = Y, Tb, Lu, and Dy).[15−17,19−21] Theoretical calculations show that the U−N bond is shorter than the U−C bond (Figure S5), which confirms that C83 is the optimized C site and N83 is the N site. Therefore, the configuration of the UCN cluster can be clearly determined, as shown in Figure 2b. The angle of U−N−C was measured as 86°, close to a right angle.

To the best of our knowledge, this encapsulated UCN cluster is the only uranium cyanide bonding motif with a triangular geometry. In the traditional U-based cyanide/nitrile and isocyanide complexes, such as $[UO_2(C_5Me_5)(CN)_3]^{2-}$ [11] and $[K(18\text{-crown}_6)]_2[(UN^*_3(CN)_2]$,[8] the UCN motif is always nearly linear. As shown in Figure 2b, the U−N and U−C distances are 2.302 and 2.520 Å, respectively, which agree with those reported for cyanide/nitrile and isocyanide complexes (2.3−2.4 Å for U−N and 2.5−2.6 Å for U−C distance).[8−14] The U−C bond distance in UCN@C_s(6)-C_{82} is similar to that of U_2C_2@I_h(7)-C_{80} (2.366−2.421 Å),[4] and it is significantly longer than the U−C distance in the previously reported U_2C@I_h(7)-C_{80} (2.033/2.028 Å).[6] Thus, U−C distances in UCN@C_s(6)-C_{82} could be assigned to a U−C single bond. Similarly, the U−N bond distance in UCN@C_s(6)-C_{82}, which is close to the U−NH_2 bond length of 2.228 Å in $[U(Tren^{TIPS})(NH_2)]$,[22] can be also assigned to a U−N single bond. Moreover, the difference between the U−C and the U−N bond lengths in UCN@C_s(6)-C_{82} is significantly higher than that of the MCN@C_s(6)-C_{82} (M = Y, Tb, Dy), which results in a more distorted UCN cluster compared to their lanthanide analogs (Table 1).[15,19,20]

Table 1. Interatomic Distances for MCN Motifs in MCN@C_s(6)-C_{82} and Traditional U-Based Coordination Compounds

sample	M−C/Å	M−N/Å	C−N/Å	ref
UCN@C_s(6)-C_{82}	2.520	2.302	1.210	this work
DyCN@C_s(6)-C_{82}	2.310	2.31	1.04	19
TbCN@C_s(6)-C_{82}	2.217	2.10	1.02	20
YCN@C_s(6)-C_{82}	2.484	2.383	0.935	15
$[\{(C_5Me_5)_2U\}_2(\mu\text{-CN})\{(\mu\text{-CN})_2Na(thf)\}_2]_\infty$	2.599	2.482	1.172	10
$[K(THF)_4][UN^*_3(CN)_2]$	2.549	2.574	1.155	13

As shown in Table 1, the C−N bond length in UCN@C_s(6)-C_{82} is 1.210 Å, which is much longer than the C−N bond in MCN@C_s(6)-C_{82} (0.935, 1.02, and 1.04 Å for Y, Tb, and Dy).[15,19,20] In fact, MCN@C_s(6)-C_{82} (M = Y, Tb, Dy) possesses a notably shorter C−N bond distance than those reported C−N triple bonds in conventional inorganic metal cyanides and cyano coordination complexes as well as for organic nitrile compounds (1.12−1.17 Å).[23−25] Though never fully explained, these studies speculated that the shrinking of the C−N bond length was due to a strong bonding between the lanthanide metal and the C/N atoms, which could be attributed to the confinement inside the interior of the carbon cage.[20] Confined in the same C_s(6)-C_{82} cage, the C−N distance for UCN, however, is surprisingly elongated compared to those for conventional uranium cyanide/nitrile compounds.[8,10−14] In U_2C_2@I_h(7)-C_{78}, the C−C bond distance of 1.26 Å is also longer than the 1.20 Å of alkynes.[4]

https://doi.org/10.1021/jacs.1c07519
J. Am. Chem. Soc. 2021, 143, 16226−16234

This suggests that the carbon cage structure may not exert a major confining effect on the C−N bond. In fact, in this case, the coordination of U with C and N effectively weakens the C−N bond. Calculations show donation bonding between the CN^- fragment and the metal; see below for details.

Theoretical Investigation. Theoretical calculations were employed to further understand the electronic structure and bonding nature of UCN@C_{82}. Starting from the X-ray coordinates, the structures of UCN@$C_s(6)$-C_{82} were optimized for doublet and quartet spin states using Kohn−Sham DFT with different hybrid and nonhybrid functionals (Table S1). It is known that C_{82} can accept two electrons, as in the case of YCN@C_{82}.[15] From an analysis of the frontier molecular orbitals (Figure S20), we have verified that there is a formal transfer of two electrons from the UCN cluster to the C_{82} cage and one electron from U to CN, i.e., $[U^{3+}(CN)^-]^{2+}@[C_s(6)\text{-}C_{82}]^{2-}$. This results in an open-shell electronic configuration with a possible doublet or quartet spin state configuration.

The most stable structures are 1a and 1b, which are almost degenerate in energy for all functionals tested, followed by 2a and 2b (also degenerate) about 23 kcal·mol^{-1} higher in energy and 21 kcal·mol^{-1} higher in Gibbs energy at 150 K (Figure S4). The difference between 1a/2a and 1b/2b, respectively, is, qualitatively, the result of exchanging C and N atoms (Figure 3a). Calculations predict a spin-quartet ground-state (GS), with a spin-doublet higher in energy by about 4 kcal·mol^{-1} for the nonhybrid functional PBE and 9 kcal·mol^{-1} for PBE0 (25% exact exchange).

A comparison of the experimental vs calculated structural parameters for UCN@$C_s(6)$-C_{82} in the different spin states for 1a and 1b (Figure S9) indicates that the PBE optimized spin-quartet structures reproduce the X-ray structural data well (Figures 2b and 3b). [Other functionals produced similar structural parameters (Figure S11).] The PBE functional predicts the 1b structure as the most stable but only 0.8 kcal·mol^{-1} lower than 1a; thus, we consider both geometries to be quasi-degenerate. The following discussion is based on the 1a structure because it better matches the experimental data.

Within the $C_s(6)$-C_{82} cage, the CN ligand adopts an η^2 (side-on) coordination. The calculated C−N distance of the UCN moiety is 1.190 Å, almost perfectly matching the experimental results. The closest U−C cage contacts are in the range of 2.42−2.60 Å, in reasonable agreement with prior reported calculated data for U_2C_2@C_{80},[4] U_2C@C_{80},[6] U_2@C_{80},[26] and U@C_{80}.[27] 2.55 Å is the average distance between U and the nearest six carbon atoms of the fullerene. The computational results are in acceptable agreement with experiments. As shown later, orbital interactions between U and CN weaken the C−N triple bond. Different orientations of the UCN cluster within the $C_s(6)$-C_{82} cage were explored in the spin-quartet calculations (Figure S10 and Table S7). Although the most stable orientation of the UCN cluster in the $C_s(6)$-C_{82} cage remains in a position where the U atom is localized close to the center of a three-hexagon carbon motif, there are other UCN orientations low in energy (at around ∼5−8 kcal·mol^{-1}), which may help to rationalize the disorder observed in the crystallographic data.

In the spin-quartet GS, assuming the transfer of two electrons to the fullerene such that the latter attains a closed shell configuration, the U center attains the formal +3 oxidation state ($5f^3$), which is supported by the spin density being mostly localized at the metal center (Figure 3c). Accordingly, the Mulliken spin population for U is ∼2.5−2.6 unpaired e (Table S1). Figure 3d shows a partial molecular orbital diagram for the ground spin-quartet state of UCN@$C_s(6)$-C_{82} with the three unpaired electrons mainly localized on the U. The natural charge and electron configuration of U from the NBO calculation are 1.1 and [core]7s(0.22)5f(3.46)-6d(0.81), respectively, showing that there is significant electron donation from the fullerene and cyanide to the uranium, which makes the resulting electronic structure qualitatively difficult to distinguish from neutral UCN with U(I) encapsulated in neutral C_{82}. In other words, the spin density favors a description as $[U]^{3+}[CN]^-@[C_s(6)\text{-}C_{82}]^{2-}$, but pronounced orbital interactions between the different moieties also allow a description in terms of U(I) if the calculated charge of the metal is associated with the oxidation number. The ambiguity regarding U(III) vs U(I) is reminiscent of the ambiguity of the assignment of $[U(C_7H_7)_2]^-$ as U(V) vs U(III).[28,29] (According to the *formal* ligand charge of −3, the later complex is assigned as U(V). However, there is extensive donation bonding in the system which brings the actual calculated uranium charge closer to +3, justifying a U(III) assignment.)

Computational Study of Molecular Bonding in UCN@ $C_s(6)$-C_{82}. Natural localized molecular orbital (NLMO) DFT analyses were performed for geometries 1a and 1b of UCN@$C_s(6)$-C_{82} and UCN^{2+}, which show overall similar chemical bonding within the UCN fragment. As stated previously, the following discussion is for 1a. The corresponding analysis for 1b is provided in the Supporting Information. For UCN@$C_s(6)$-C_{82}, there are three spin pairs of NLMOs, one σ and two π, describing the triple bond of CN^- (see Figure 4). The π NLMOs display some three-center character, that is, delocalization toward U, with weights between 4% and 6% from U based 6d−5f hybrids. Furthermore, the C- and N-centered lone-pair NLMOs have sizable weights at U, between 7% and 11%. On the basis of this NLMO delocalization onto the U center, we assign donation bonding between the CN^- fragment and the metal center. The effect is relatively weak for

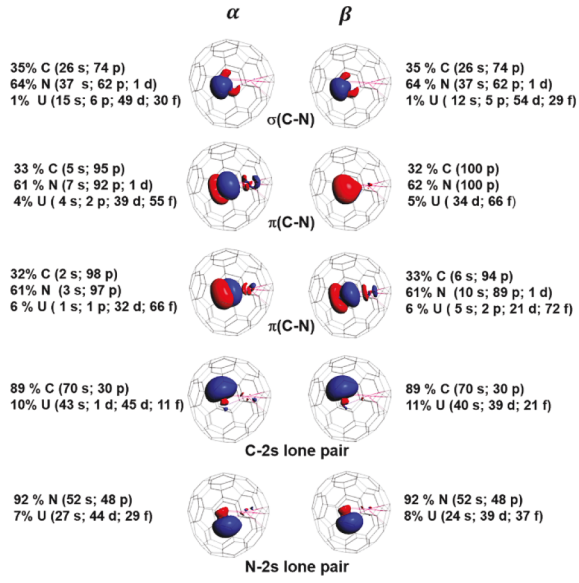

Figure 4. NLMO isosurfaces (±0.03 au) and atomic orbital weight compositions (in %) obtained from natural bond orbital analysis of the ZORA/DFT/PBE quartet state of UCN@$C_s(6)$-C_{82}. α- and β-spin orbitals are shown separately.

https://doi.org/10.1021/jacs.1c07519
J. Am. Chem. Soc. 2021, 143, 16226−16234

the individual NLMOs, but in aggregate the donation bonding from cyanide to U is seen to be quite pronounced (Figure 4). Because the donation bonding not only involves the ligand lone pairs but also bonding orbitals, it effectively weakens the CN^- triple bond, which correlates with the elongated C−N distance noted earlier. In the calculations, relative to free CN^-, the CN stretching vibrational frequency is lowered by about 60 wavenumbers for UCN@C_{82} and by about 110 wavenumbers for isolated UCN^{2+} in side-on structure. The frequency-lowering supports the weakening of the CN bond assigned via the NLMO analysis. The occupations of the π^* NBOs of CN^- are negligible, and therefore a back-donation mechanism can be ruled out.

Some NLMOs of the carbon cage also have density at U; the ones with U weights larger than 4% are plotted in Figure S16. The analysis also indicates that uranium donates α-spin density to the carbon cage, hence the U spin population of less than 3, which compensates somewhat for the donation bonding from the CN^- fragment in terms of the overall U electron count.

Molecular Structure and Bonding of UCN. Neutral UCN was optimized for different spin states (Figure S7 and Table S4). Formally, UCN has U(I), with five 5f occupations. For this reason, we considered doublet, quartet, and sextet spin states. The spin-quartet ground-state geometry is predicted to be the lowest in energy, with the spin-sextet triangle structure lying higher in energy by 6.4 kcal·mol^{-1} and the spin-sextet linear structure by 7.5 kcal·mol^{-1}. The spin-doublet ground-state was predicted at 15.2 kcal·mol^{-1}. UCN adopts a linear shape in the spin-quartet ground-state.

Inside the fullerene, we assigned the electronic structure to UCN^{2+}, with U(III), not considering donation bonding. Isolated UCN^{2+} was therefore also optimized for doublet and quartet spin states in linear and triangular arrangements (Figure S6 and Table S3). The spin-quartet ground-state linear structure turned out to be the lowest in energy, followed by the spin-quartet triangular arrangement at 3.2 kcal·mol^{-1}. Evidently, the interaction with the $C_s(6)$-C_{82} causes UCN^{2+} to adopt the η^2 (side-on) coordination of the cyanide. Such an unprecedented triangular configuration of cyanide clusters provides a new concept for coordination chemistry and can also help us to better appreciate the wide-ranging bonding ability of uranium.

As for UCN@$C_s(6)$-C_{82}, the formal triple bond of CN^- for UCN^{2+} is described by three spin pairs of bonding NLMOs, one σ and two π, and the lone pair NLMOs on C and N (see Figure 5). There is, as in the encapsulated species, some three-center character of the π NLMOs, and the C lone pair NLMO particularly strongly contributes to the donation bonding in the geometric arrangement adopted by the free UCN^{2+} species.

Spectroscopic Characterizations. The structure of UCN@$C_s(6)$-C_{82} was further characterized by UV−vis−NIR absorption spectroscopy. The absorption spectrum of endohedral metallofullerene is generally dominated by the $\pi \rightarrow \pi^*$ excitation of the carbon cage π system.[31] Therefore, in principle, regardless of the encapsulated metal, the spectra of EMFs with the same carbon cage isomers and same formal charge state are generally very similar. Figure 6a shows three peaks at 499, 706, and 1055 nm. These absorbances are almost identical to those for MCN@$C_s(6)$-C_{82} (M = Tb, Y, Lu, and Dy),[15−17,19,20] suggestive of a similar electronic structure, $(MCN)^{2+}@{C_{82}}^{2-}$.

UCN@$C_s(6)$-C_{82} was also characterized by low energy Raman spectroscopy, as shown in Figure 6b. Three sharp peaks

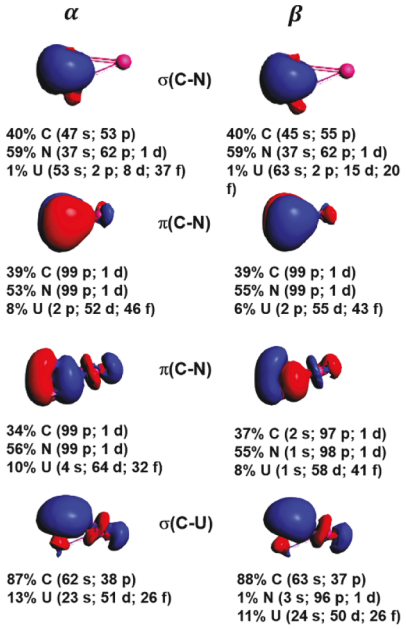

Figure 5. NLMO isosurfaces (±0.03 au) and atomic orbital weight compositions (in %) obtained from a natural bond orbital analysis of the ZORA/DFT/PBE quartet state obtained for UCN^{2+}. α- and β-spins orbitals are shown separately.

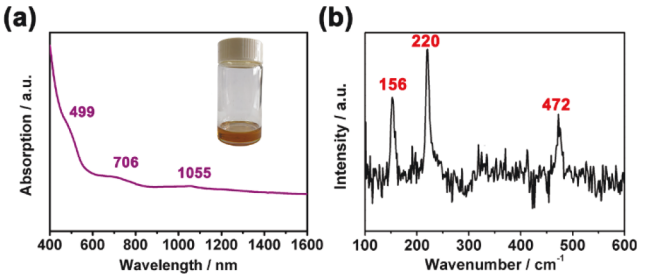

Figure 6. (a) UV−vis−NIR spectrum of UCN@$C_s(6)$-C_{82} in CS_2. The inset shows a photograph of ca. 0.5 mg of UCN@$C_s(6)$-C_{82} dissolved in 5 mL of CS_2 solution. (b) Low-energy Raman spectra of UCN@$C_s(6)$-C_{82} at 785 nm excitation.

were observed at 156, 220, and 472 cm^{-1}. The peak at 156 cm^{-1} can be assigned to the metal-to-cage vibrational mode,[31] which is close to those for U@C_1(17418)-C_{76} (153 cm^{-1}) and U@C_1(28324)-C_{80} (145 cm^{-1}),[27] suggesting similar metal−cage interactions for U-based EMFs. In addition, theoretical calculations determined that the vibrational peaks (220 and 472 cm^{-1}) in the range of 200−500 cm^{-1} can be assigned to the cage vibrational mode, similar to those of Ce@$C_s(6)$-C_{82}[32] (221 and 430 cm^{-1}) and Pr@$C_s(6)$-C_{82} (227 and 432 cm^{-1}), in good agreement with the crystallographic analysis.[33]

Electrochemical Study of UCN@$C_s(6)$-C_{82}. The cyclic voltammogram of UCN@$C_s(6)$-C_{82} measured in *o*-dichlorobenzene (*o*-DCB) with tetrabutylammonium hexafluorophosphate ($TBAPF_6$) as supporting electrolyte is shown in Figure 7, and the characteristic redox potentials are summarized in Table 2, along with values for other C_{82}-based EMFs. In the cathodic region, UCN@$C_s(6)$-C_{82} exhibits four reversible reduction steps at −0.57, −0.97, −1.71, and −1.89 V, respectively, showing similar redox behavior to those of the lanthanide homologues.[15−17,19,20] The separation between the second and third reduction steps (0.74 V) is much larger than

https://doi.org/10.1021/jacs.1c07519
J. Am. Chem. Soc. 2021, 143, 16226−16234

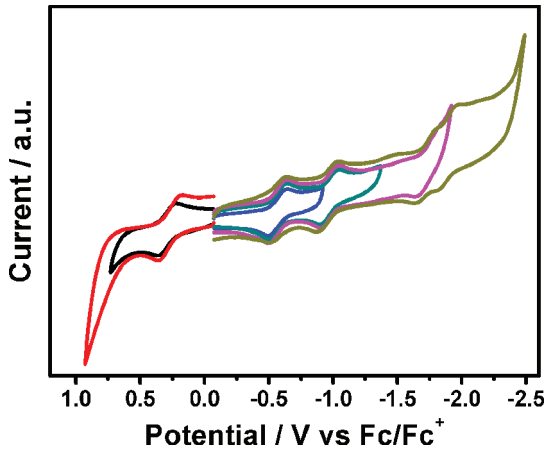

Figure 7. Cyclic voltammograms of UCN@C_s(6)-C_{82}, measured in a 0.05 M (n-Bu)$_4$NPF$_6$/o-DCB solution. Ferrocene (Fc) was added as the internal potential standard, and TBAPF$_6$ was added as supporting electrolyte. Scan rate: 100 mV/s.

those of the first−second/third−fourth reduction steps (0.40 and 0.18 V, respectively), a characteristic feature for the EMFs exhibiting two electron transfer between the clusters and the cages, such as MCN@C_{82} (M = Tb, Y, Lu, and Dy)[15−17,19−21] as well as Yb@C_s(6)-C_{82},[30] in agreement with the assigned electronic configuration of $[U^{3+}(CN)^-]^{2+}$@$[C_s(6)\text{-}C_{82}]^{2-}$. On the other hand, Table 2 shows that the first oxidation potential of UCN@C_s(6)-C_{82} (0.29 V) is considerably shifted compared to that of MCN@C_s(6)-C_{82} (M = Tb, Y, Lu, and Dy), resulting in a notably smaller electrochemical band gap.[15−17,19,20] This could be attributed to the fact that UCN@C_s(6)-C_{82} has an open shell structure while all of the MCN@C_s(6)-C_{82} (M = Tb, Y, Lu, and Dy) have closed shell electronic structures.

CONCLUSION

A novel cyanide clusterfullerene, UCN@C_s(6)-C_{82}, was successfully synthesized and fully characterized by a variety of experimental and theoretical techniques. Crystallographic analysis reveals a triangular uranium with an unprecedented η^2 (side-on) coordination with cyanide, which has never been observed for traditional U-based cyanide/nitrile and isocyanide complexes, stabilized inside a C_{82} fullerene cage. The combined experimental and theoretical investigation shows that the system can be described as $[U^{3+}(CN)^-]^{2+}$@$[C_s(6)\text{-}C_{82}]^{2-}$, with U adopting an oxidation state of +III and a two-electron transfer from UCN to C_{82}. Theoretical analysis predicted a spin-quartet ground-state and further revealed substantial donation bonding between the CN^- fragment and the metal center, as well as some α-spin density donation from uranium to the carbon cage. The significant donation bonding from the fullerene and cyanide to the uranium makes the resulting system qualitatively difficult to distinguish from neutral UCN with U(I) encapsulated in neutral C_{82}. The theoretical analysis supports both interpretations and is reminiscent of other ambiguous cases known in uranium chemistry, as noted earlier. The discovery of this unprecedented triangular uranium cyanide cluster provides new insights in coordination chemistry and can also help us better understand the diverse bonding motifs adopted by the U element.

EXPERIMENTAL DETAILS

Spectroscopic and Electrochemical Studies. The positive-ion mode matrix-assisted laser desorption ionization time-of-flight (MALDI-TOF) (Bruker, Germany) was employed for the mass characterization. The UV−vis−NIR spectra of the purified UCN@C_s(6)-C_{82} were measured in a CS_2 solution with a Cary 5000 UV−vis−NIR spectrophotometer (Agilent, USA). The Raman spectra were obtained using a Horiba Lab RAM HR Evolution Raman spectrometer using a laser at 785 nm. Cyclic voltammetry (CV) results were obtained in o-dichlorobenzene using a CHI-660E instrument. A conventional three-electrode cell consisting of a platinum counter electrode, a glassy carbon working electrode, and a silver reference electrode was used for the measurements. (n-Bu)$_4$NPF$_6$ (0.05 M) was used as supporting electrolyte. The CV data were measured at the scan rate of 100 mV/s.

X-ray Crystallographic Study. The black block crystals of UCN@C_s(6)-C_{82} were obtained by slow diffusion of the a CS_2 solution of the corresponding metallofullerene compounds into the a benzene solution of [Ni^{II}(OEP)]. Single-crystal X-ray data of UCN@C_s(6)-C_{82} were collected at 150 K on a diffractometer (APEX II; Bruker D8 Venture) equipped with a CCD collector. The multiscan method was used for absorption correction. The structures were solved using the intrinsic phasing methods[34] and refined on F^2 using full-matrix least-squares using the SHELXL2018 crystallographic software packages.[35] Hydrogen atoms were inserted at calculated positions and constrained with isotropic thermal parameters.

Crystal data for UCN@C_s(6)-C_{82}·[Ni^{II}(OEP)]·2C_6H_6. M_r = 1934.66, 0.15 mm × 0.12 mm × 0.10 mm, monoclinic, $C2/m$ (No. 12), a = 25.3779(6) Å, b = 15.0813(3) Å, c = 19.9914(5) Å, α = 90°, β = 94.6750(10)°, γ = 90°, V = 7625.9(3) Å^3, Z = 4, ρ_{calcd} = 1.739 g·cm^{-3}, μ(Mo Kα) = 6.789 mm^{-1}, θ = 3.49−74.52, T = 150.0 K, R_1 = 0.0878, wR_2 = 0.2505 for all data; R_1 = 0.0829, wR_2 = 0.2437 for 7381 reflections ($I \geqslant 2\sigma(I)$) with 1045 parameters. Goodness-of-fit indicator, 1.046. Maximum residual electron density, 1.174 e Å^{-3}.

Computational Details. Kohn−Sham (KS) density functional theory (DFT) was performed using the Amsterdam Density Functional (ADF, version 2017) package.[36] The Perdew−Burke−Ernzerhof (PBE)[37] functional with an all-electron triple-ζ polarized (TZP) Slater-type orbital (STO) basis sets[38,39] was employed for geometry optimizations and electronic structure analyses. Relativistic effects were considered by means of the scalar relativistic (SR) zero-

Table 2. Redox Potential (V vs Fc/Fc$^+$) and Electrochemical Gaps ($\Delta E_{gap,EC}$/V) of UCN@C_s(6)-C_{82} and Other Reported C_{82}-Based EMFs[a]

sample	$E^{+/0}$	$E^{0/-}$	$E^{-/2-}$	$E^{2-/3-}$	$E^{3-/4-}$	$\Delta E_{gap,EC}$/V	ref
UCN@C_s(6)-C_{82}	0.29	−0.57	−0.97	−1.71	−1.89	0.86	this work
YCN@C_s(6)-C_{82}	0.56	−0.59	−0.84	−1.76	−1.92	1.15	15
TbCN@C_s(6)-C_{82}	0.55	−0.59	−0.84	−1.77	−1.92	1.14	20
LuCN@C_s(6)-C_{82}	0.52	−0.58	−0.90	−1.69	−1.86	1.10	16
DyCN@C_s(6)-C_{82}	0.56	−0.58	−0.84	−1.77	−1.92	1.14	19
Yb@C_s(6)-C_{82}	0.34	−0.62	−0.92	−1.81	−2.01	0.96	30

[a]All redox steps are reversible, and the potential values in the table are half-wave potentials. $\Delta E_{gap,EC}$/V = $E^{+/0} - E^{0/-}$.

https://doi.org/10.1021/jacs.1c07519
J. Am. Chem. Soc. 2021, 143, 16226−16234

order regular approximation (ZORA).[40] "D3" dispersion corrections[41,42] were included in the calculations. Test calculations with different functionals were also performed, showing no significant differences. Additional optimizations were carried out with the Gaussian (G16) package,[43] the PBE functional, and Gaussian-type orbital (GTO) basis sets as follows: 6-31G(d,p) for C and the SDD basis sets with a matching scalar relativistic effective core potential for U, as provided by the G16 basis set library.[44] These calculations produced equivalent structural parameters and spin state energetics as the ADF calculations. Selected optimized systems were subjected to natural localized molecular orbital (NLMO) bonding analyses, carried out with NBO6.[45]

The Raman spectrum was calculated with G16, the PBE functional, and the same basis sets used in the optimization. The optimization followed by the frequency and Raman intensity calculations was performed for UCN@C_s(6)-C_{82}.

■ ASSOCIATED CONTENT

Supporting Information

The Supporting Information is available free of charge at https://pubs.acs.org/doi/10.1021/jacs.1c07519.

HPLC profiles for the separation of UCN@C_s(6)-C_{82}, experimental details, and complementary computational results (PDF)

Accession Codes

CCDC 2050570 contains the supplementary crystallographic data for this paper. These data can be obtained free of charge via www.ccdc.cam.ac.uk/data_request/cif, or by emailing data_request@ccdc.cam.ac.uk, or by contacting The Cambridge Crystallographic Data Centre, 12 Union Road, Cambridge CB2 1EZ, UK; fax: +44 1223 336033.

■ AUTHOR INFORMATION

Corresponding Authors

Jochen Autschbach − *Department of Chemistry, University at Buffalo, State University of New York, Buffalo, New York 14260-3000, United States;* orcid.org/0000-0001-9392-877X; Email: jochena@buffalo.edu

Ning Chen − *College of Chemistry, Chemical Engineering and Materials Science, and State Key Laboratory of Radiation Medicine and Protection, Soochow University, Suzhou, Jiangsu 215123, P. R. China;* orcid.org/0000-0002-9405-6229; Email: chenning@suda.edu.cn

Authors

Qingyu Meng − *College of Chemistry, Chemical Engineering and Materials Science, and State Key Laboratory of Radiation Medicine and Protection, Soochow University, Suzhou, Jiangsu 215123, P. R. China*

Laura Abella − *Department of Chemistry, University at Buffalo, State University of New York, Buffalo, New York 14260-3000, United States;* orcid.org/0000-0003-2188-248X

Wei Yang − *College of Chemistry, Chemical Engineering and Materials Science, and State Key Laboratory of Radiation Medicine and Protection, Soochow University, Suzhou, Jiangsu 215123, P. R. China*

Yang-Rong Yao − *Department of Chemistry and Biochemistry, University of Texas at El Paso, El Paso, Texas 79968, United States*

Xinye Liu − *College of Chemistry, Chemical Engineering and Materials Science, and State Key Laboratory of Radiation Medicine and Protection, Soochow University, Suzhou, Jiangsu 215123, P. R. China*

Jiaxin Zhuang − *College of Chemistry, Chemical Engineering and Materials Science, and State Key Laboratory of Radiation Medicine and Protection, Soochow University, Suzhou, Jiangsu 215123, P. R. China*

Xiaomeng Li − *College of Chemistry, Chemical Engineering and Materials Science, and State Key Laboratory of Radiation Medicine and Protection, Soochow University, Suzhou, Jiangsu 215123, P. R. China*

Luis Echegoyen − *Department of Chemistry and Biochemistry, University of Texas at El Paso, El Paso, Texas 79968, United States;* orcid.org/0000-0003-1107-9423

Complete contact information is available at: https://pubs.acs.org/10.1021/jacs.1c07519

Author Contributions

‖Q.M., L.A., and W.Y. contributed equally to this work.

Notes

The authors declare no competing financial interest.

■ ACKNOWLEDGMENTS

N.C. thanks the National Science Foundation China (Grants NSFC 91961109 and NSFC 51302178), the Natural Science Foundation of Jiangsu Province (Grant BK20200041), and the Priority Academic Program Development of Jiangsu Higher Education Institutions (PAPD). J.A. acknowledges support from the U.S. Department of Energy, Office of Basic Energy Sciences, Heavy Element Chemistry Program, under Grant DE-SC0001136. We thank the Center for Computational Research (CCR) at the University at Buffalo for providing computational resources. L.E. thanks the NSF for the generous support of this work under Grant CHE-1801317. The Robert A. Welch Foundation is also gratefully acknowledged for an Endowed Chair to L.E. (Grant AH-0033).

■ REFERENCES

(1) Kelley, M. P.; Su, J.; Urban, M.; Luckey, M.; Batista, E. R.; Yang, P.; Shafer, J. C. On the Origin of Covalent Bonding in Heavy Actinides. *J. Am. Chem. Soc.* **2017**, *139* (29), 9901−9908.

(2) Hu, S. X.; Li, W. L.; Lu, J. B.; Bao, J. L.; Yu, H. S.; Truhlar, D. G.; Gibson, J. K.; Marcalo, J.; Zhou, M.; Riedel, S.; Schwarz, W. H. E.; Li, J. On the Upper Limits of Oxidation States in Chemistry. *Angew. Chem., Int. Ed.* **2018**, *57* (12), 3242−3245.

(3) Qiu, J.; Burns, P. C. Clusters of actinides with oxide, peroxide, or hydroxide bridges. *Chem. Rev.* **2013**, *113* (2), 1097−1120.

(4) Zhuang, J.; Abella, L.; Sergentu, D. C.; Yao, Y. R.; Jin, M.; Yang, W.; Zhang, X.; Li, X.; Zhang, D.; Zhao, Y.; Li, X.; Wang, S.; Echegoyen, L.; Autschbach, J.; Chen, N. Diuranium(IV) Carbide Cluster U_2C_2 Stabilized Inside Fullerene Cages. *J. Am. Chem. Soc.* **2019**, *141* (51), 20249−20260.

(5) Cai, W.; Chen, C. H.; Chen, N.; Echegoyen, L. Fullerenes as Nanocontainers That Stabilize Unique Actinide Species Inside: Structures, Formation, and Reactivity. *Acc. Chem. Res.* **2019**, *52* (7), 1824−1833.

(6) Zhang, X.; Li, W.; Feng, L.; Chen, X.; Hansen, A.; Grimme, S.; Fortier, S.; Sergentu, D. C.; Duignan, T. J.; Autschbach, J.; Wang, S.; Wang, Y.; Velkos, G.; Popov, A. A.; Aghdassi, N.; Duhm, S.; Li, X.; Li, J.; Echegoyen, L.; Schwarz, W. H. E.; Chen, N. A diuranium carbide cluster stabilized inside a C_{80} fullerene cage. *Nat. Commun.* **2018**, *9* (1), 2753−2760.

(7) Berthet, J.-C.; Thuéry, P.; Ephritikhine, M. Advances in f-element cyanide chemistry. *Dalton Trans.* **2015**, *44* (17), 7727−7742.

(8) Herve, A.; Bouzidi, Y.; Berthet, J. C.; Belkhiri, L.; Thuery, P.; Boucekkine, A.; Ephritikhine, M. U-CN versus Ce-NC coordination in trivalent complexes derived from $M[N(SiMe_3)_2]_3$ (M = Ce, U). *Inorg. Chem.* **2014**, *53* (13), 6995−7013.

(9) Maynadié, J.; Berthet, J.-C.; Thuéry, P.; Ephritikhine, M. Bent and Linear Uranium(IV) Metallocenes with Terminal and Bridging Cyanide Ligands. *Organometallics* **2007**, *26* (18), 4585−4591.
(10) Maynadié, J.; Berthet, J.-C.; Thuéry, P.; Ephritikhine, M. Cyanide Metallocenes of Trivalent f-Elements. *Organometallics* **2007**, *26* (10), 2623−2629.
(11) Maynadie, J.; Berthet, J. C.; Thuery, P.; Ephritikhine, M. The first cyclopentadienyl complex of uranyl. *Chem. Commun.* **2007**, *5*, 486−488.
(12) Benaud, O.; Berthet, J. C.; Thuery, P.; Ephritikhine, M. Iodide, azide, and cyanide complexes of (N,C), (N,N), and (N,O) metallacycles of tetra- and pentavalent uranium. *Inorg. Chem.* **2011**, *50* (23), 12204−12214.
(13) Herve, A.; Bouzidi, Y.; Berthet, J. C.; Belkhiri, L.; Thuery, P.; Boucekkine, A.; Ephritikhine, M. U(III)-CN versus U(IV)-NC coordination in tris(silylamide) complexes. *Inorg. Chem.* **2015**, *54* (5), 2474−2490.
(14) Zi, G.; Jia, L.; Werkema, E. L.; Walter, M. D.; Gottfriedsen, J. P.; Andersen, R. A. Preparation and Reactions of Base-Free Bis(1,2,4-tri-tert-butylcyclopentadienyl)uranium Oxide, Cp′$_2$UO. *Organometallics* **2005**, *24* (17), 4251−4264.
(15) Yang, S.; Chen, C.; Liu, F.; Xie, Y.; Li, F.; Jiao, M.; Suzuki, M.; Wei, T.; Wang, S.; Chen, Z.; Lu, X.; Akasaka, T. An improbable monometallic cluster entrapped in a popular fullerene cage: YCN@C_s(6)-C_{82}. *Sci. Rep.* **2013**, *3*, 1487−1492.
(16) Shen, W.; Hu, Z.; Yu, P.; Wei, Z.; Jin, P.; Shi, Z.; Lu, X. An experimental and theoretical study of LuNC@$C_{76,82}$ revealing a cage-cluster selection rule. *Inorg. Chem. Front.* **2020**, *7* (23), 4563−4571.
(17) Liu, F.; Wang, S.; Gao, C.-L.; Deng, Q.; Zhu, X.; Kostanyan, A.; Westerström, R.; Jin, F.; Xie, S.-Y.; Popov, A. A.; Greber, T.; Yang, S. Mononuclear Clusterfullerene Single-Molecule Magnet Containing Strained Fused-Pentagons Stabilized by a Nearly Linear Metal Cyanide Cluster. *Angew. Chem., Int. Ed.* **2017**, *56* (7), 1830−1834.
(18) Guan, R.; Chen, M.; Xin, J.; Xie, X.-M.; Jin, F.; Zhang, Q.; Xie, S.-Y.; Yang, S. Capturing the Missing Carbon Cage Isomer of C_{84} via Mutual Stabilization of a Triangular Monometallic Cyanide Cluster. *J. Am. Chem. Soc.* **2021**, *143* (21), 8078−8085.
(19) Yang, S.; Xin, J.; Jin, F.; Guan, R.; Chen, M.; Xie, X.-M.; Zhang, Q.; Xie, S.-Y. Ancient pigment to treasure: Prussian blue as a cheap solid cyanide/nitrogen dual-source affording high-yield syntheses of pricey endohedral clusterfullerenes. *Inorg. Chem. Front.* **2021**, *8*, 1719−1726.
(20) Liu, F.; Gao, C. L.; Deng, Q.; Zhu, X.; Kostanyan, A.; Westerstrom, R.; Wang, S.; Tan, Y. Z.; Tao, J.; Xie, S. Y.; Popov, A. A.; Greber, T.; Yang, S. Triangular Monometallic Cyanide Cluster Entrapped in Carbon Cage with Geometry-Dependent Molecular Magnetism. *J. Am. Chem. Soc.* **2016**, *138* (44), 14764−14771.
(21) Liu, F.; Wang, S.; Guan, J.; Wei, T.; Zeng, M.; Yang, S. Putting a terbium-monometallic cyanide cluster into the C_{82} fullerene cage: TbCN@C_2(5)-C_{82}. *Inorg. Chem.* **2014**, *53* (10), 5201−5205.
(22) King, D. M.; Tuna, F.; McInnes, E. J.; McMaster, J.; Lewis, W.; Blake, A. J.; Liddle, S. T. Isolation and characterization of a uranium(VI)-nitride triple bond. *Nat. Chem.* **2013**, *5* (6), 482−488.
(23) Harris, K. J.; Wasylishen, R. E. A 13C and 15N Solid-State NMR Study of Structural Disorder and Aurophilic Bonding in AuI and AuIII Cyanide Complexes. *Inorg. Chem.* **2009**, *48* (5), 2316−2332.
(24) Orpen, A. G.; Brammer, L.; Allen, F. H.; Kennard, O.; Watson, D. G.; Taylor, R. Supplement. Tables of bond lengths determined by X-ray and neutron diffraction. Part 2. Organometallic compounds and co-ordination complexes of the d- and f-block metals. *J. Chem. Soc., Dalton Trans.* **1989**, *12*, S1−S83.
(25) Stevens, P. A.; Madix, R. J.; Stöhr, J. The bonding of acetonitrile and CH_2CN on Ag(110) determined by near edge x-ray absorption fine structure: Evidence for π-donor bonding and azimuthal ordering. *J. Chem. Phys.* **1989**, *91* (7), 4338−4345.
(26) Zhang, X.; Wang, Y.; Morales-Martinez, R.; Zhong, J.; de Graaf, C.; Rodriguez-Fortea, A.; Poblet, J. M.; Echegoyen, L.; Feng, L.; Chen, N. U_2@I_h(7)-C_{80}: Crystallographic Characterization of a Long-Sought Dimetallic Actinide Endohedral Fullerene. *J. Am. Chem. Soc.* **2018**, *140* (11), 3907−3915.
(27) Cai, W.; Abella, L.; Zhuang, J.; Zhang, X.; Feng, L.; Wang, Y.; Morales-Martinez, R.; Esper, R.; Boero, M.; Metta-Magana, A.; Rodriguez-Fortea, A.; Poblet, J. M.; Echegoyen, L.; Chen, N. Synthesis and Characterization of Non-Isolated-Pentagon-Rule Actinide Endohedral Metallofullerenes U@C_1(17418)-C_{76}, U@C_1(28324)-C_{80}, and Th@C_1(28324)-C_{80}: Low-Symmetry Cage Selection Directed by a Tetravalent Ion. *J. Am. Chem. Soc.* **2018**, *140* (51), 18039−18050.
(28) Li, J.; Bursten, B. E. Electronic Structure of Cycloheptatrienyl Sandwich Compounds of Actinides: An(η^7-C_7H_7)$_2$ (An = Th, Pa, U, Np, Pu, Am). *J. Am. Chem. Soc.* **1997**, *119* (38), 9021−9032.
(29) Sergentu, D.-C.; Gendron, F.; Autschbach, J. Similar ligand−metal bonding for transition metals and actinides? $5f^1$ U-$(C_7H_7)^{2-}$versus $3d^n$ metallocenes. *Chem. Sci.* **2018**, *9* (29), 6292−6306.
(30) Popov, A. A.; Yang, S.; Dunsch, L. Endohedral fullerenes. *Chem. Rev.* **2013**, *113* (8), 5989−6113.
(31) Shibata, K.; Rikiishi, Y.; Hosokawa, T.; Haruyama, Y.; Kubozono, Y.; Kashino; Uruga, T.; Fujiwara, A.; Kitagawa, H.; Takano; Iwasa, Y. Structural and electronic properties of Ce@C_s(6)-C_{82}. *Phys. Rev. B: Condens. Matter Mater. Phys.* **2003**, *68* (9), 094104.
(32) Hosokawa, T.; Fujiki, S.; Kuwahara, E.; Kubozono, Y.; Kitagawa, H.; Fujiwara, A.; Takenobu, T.; Iwasa, Y. Electronic properties for the C_{2v} and C_s isomers of Pr@C_{82} studied by Raman, resistivity and scanning tunneling microscopy/spectroscopy. *Chem. Phys. Lett.* **2004**, *395* (1), 78−81.
(33) Lu, X.; Slanina, Z.; Akasaka, T.; Tsuchiya, T.; Mizorogi, N.; Nagase, S. Yb@C_{2n} (n = 40, 41, 42): New Fullerene Allotropes with Unexplored Electrochemical Properties. *J. Am. Chem. Soc.* **2010**, *132* (16), 5896−5905.
(34) Dolomanov, O. V.; Bourhis, L. J.; Gildea, R. J.; Howard, J. A. K.; Puschmann, H. OLEX2: a complete structure solution, refinement and analysis program. *J. Appl. Crystallogr.* **2009**, *42* (2), 339−341.
(35) Sheldrick, G. Crystal structure refinement with SHELXL. *Acta Crystallogr., Sect. C: Struct. Chem.* **2015**, *71* (1), 3−8.
(36) Baerends, E. J.; Ziegler, T.; Atkins, A.; Autschbach, J.; Bashford, D.; Baseggio, O.; Bérces, A.; Bickelhaupt, F.; Bo, C.; Boerritger, P. *ADF2017, SCM, Theoretical Chemistry*; Vrije Universiteit: Amsterdam, The Netherlands, 2017.
(37) Perdew, J. P.; Burke, K.; Ernzerhof, M. Generalized Gradient Approximation Made Simple [Phys. Rev. Lett. 77, 3865 (1996)]. *Phys. Rev. Lett.* **1997**, *78* (7), 1396−1396.
(38) Schlegel, H. B. Potential energy curves using unrestricted Moller−Plesset perturbation theory with spin annihilation. *J. Chem. Phys.* **1986**, *84* (8), 4530−4534.
(39) Perdew, J. P. Density-functional approximation for the correlation energy of the inhomogeneous electron gas. *Phys. Rev. B: Condens. Matter Mater. Phys.* **1986**, *33* (12), 8822−8824.
(40) Lenthe, E. v.; Baerends, E. J.; Snijders, J. G. Relativistic regular two-component Hamiltonians. *J. Chem. Phys.* **1993**, *99* (6), 4597−4610.
(41) Grimme, S.; Antony, J.; Ehrlich, S.; Krieg, H. A consistent and accurate ab initio parametrization of density functional dispersion correction (DFT-D) for the 94 elements H-Pu. *J. Chem. Phys.* **2010**, *132* (15), 154104.
(42) Grimme, S.; Ehrlich, S.; Goerigk, L. Effect of the damping function in dispersion corrected density functional theory. *J. Comput. Chem.* **2011**, *32* (7), 1456−1465.
(43) Frisch, M.; Trucks, G.; Schlegel, H.; Scuseria, G.; Robb, M.; Cheeseman, J.; Scalmani, G.; Barone, V.; Petersson, G.; Nakatsuji, H.; et al. *Gaussian 16*, revision B.01; Gaussian, Inc.: Wallingford, CT, 2016.
(44) Cao, X.; Dolg, M. Segmented contraction scheme for small-core lanthanide pseudopotential basis sets. *J. Mol. Struct.: THEOCHEM* **2002**, *581* (1), 139−147.

(45) Glendening, E. D.; Landis, C. R.; Weinhold, F. NBO 6.0: Natural bond orbital analysis program. *J. Comput. Chem.* **2013**, *34* (16), 1429−1437.

https://doi.org/10.1021/jacs.1c07519
J. Am. Chem. Soc. 2021, 143, 16226−16234